ChemComm

FEATURE ARTICLE

View Article Online
View Journal

Check for updates

Cite this: DOI: 10.1039/c8cc01202d

Integrated nanozymes: facile preparation and biomedical applications

Jiangjiexing Wu,†[ab] Sirong Li†[a] and Hui Wei *[abc]

Nanozymes have been viewed as the next generation of artificial enzymes due to their low cost, large specific surface area, and good robustness under extreme conditions. However, the moderate activity and limited selectivity of nanozymes have impeded their usage. To overcome these shortcomings, integrated nanozymes (INAzymes) have been developed by encapsulating two or more different biocatalysts (*e.g.*, natural oxidases and peroxidase mimics) together within confined frameworks. On the one hand, with the assistance of natural enzymes, INAzymes are capable of specifically recognizing targets. On the other hand, nanoscale confinement brought about by integration significantly enhances the cascade reaction efficiency. In this Feature Article, we highlight the newly developed INAzymes, covering from synthetic strategies to versatile applications in biodetection and therapeutics. Moreover, it is predicted that INAzymes with superior activities, specificity, and stability will enrich the research of nanozymes and pave new ways in designing multifunctional nanozymes.

Received 10th February 2018,
Accepted 13th March 2018

DOI: 10.1039/c8cc01202d

rsc.li/chemcomm

Published on 13 March 2018. Downloaded by NANJING UNIVERSITY on 22/04/2018 09:59:00.

1. Introduction

Developing robust enzyme mimics has been considered as an ideal solution to overcome natural enzyme limitations, such as laborious production, low stability, and high cost. Among the developed enzyme mimics, nanomaterials with enzyme mimicking activities (termed as nanozymes) have received considerable attention due to the burgeoning development of nanotechnology.[1–7] A variety of nanomaterials have been explored to mimic enzymes, including noble metals,[8–13] transition metal oxides,[14–18] carbon materials[19–22] and so on.[23–28] Until now, nanozymes have found broad applications, ranging from bioanalysis[14,29–35] and diagnosis[36,37] to tissue engineering[38,39] and environmental protection.[40,41]

Despite the remarkable achievements accomplished in the last few decades, moderate activity and limited selectivity have impeded the further use of nanozymes. Early studies on glucose detection using nanozymes indicated that high selectivity could be achieved by coupling a nanozyme with a natural enzyme – glucose oxidase (GOx) – for glucose detection.[29,42–45] However, such coupled reactions still suffer from a limited overall efficiency because of the spatially separated reactions. Hence, rational design is of great need to advance high performance nanozymes with both improved selectivity and efficiency.

In this regard, nature has evolved a highly elegant strategy to perform cascade reactions by confining sequential enzymes within subcellular compartments. Such a sophisticated confinement enhances the overall efficiency of the cascade reactions by (a) providing a high local concentration of enzymes and substrates, (b) enabling efficient mass transfer, and (c) minimizing intermediate decomposition. These enhancement phenomena are collectively called "confinement effects" or "nanoscale proximity effects". Various catalytic reactions verified the superiority of the aforementioned effects.[46–49] For instance, Travis *et al.* promoted the efficiency of a 10-step enzymatic tandem reaction to convert glucose into lactate by immobilizing the enzymes on silica nanoparticles (NPs).[50] Bao and co-workers have used a bioinspired strategy to develop interface-confined catalysts for a series of reactions (such as carbon monoxide oxidation and the oxygen reduction reaction).[51]

Such great successes encouraged us and others to apply the "nanoscale proximity effects" to designing integrated nanozymes (INAzymes) (Fig. 1 and Table 1). By encapsulating natural enzymes and nanozymes together within a nanoscaled framework, the designed INAzymes aim to overcome the moderate activity and limited selectivity issues of nanozymes. Numerous INAzymes have been developed and used in versatile applications. To highlight the progress of the INAzymes, this article first discusses the different synthetic strategies for INAzymes. Then, their representative biomedical applications are illustrated. Finally, the perspectives that may advance nanozyme research are discussed.

[a] *Department of Biomedical Engineering, College of Engineering and Applied Sciences, Nanjing National Laboratory of Microstructures, Nanjing University, Nanjing, Jiangsu, 210093, China. E-mail: weihui@nju.edu.cn; Web: http://weilab.nju.edu.cn; Fax: +86-25-83594648; Tel: +86-25-83593272*

[b] *State Key Laboratory of Coordination Chemistry, School of Chemistry and Chemical Engineering, Nanjing University, Nanjing, Jiangsu, 210093, China*

[c] *State Key Laboratory of Analytical Chemistry for Life Science, School of Chemistry and Chemical Engineering, Nanjing University, Nanjing, Jiangsu, 210093, China*

† These two authors contributed equally.

Published on 13 March 2018. Downloaded by NANJING UNIVERSITY on 22/04/2018 09:59:00.

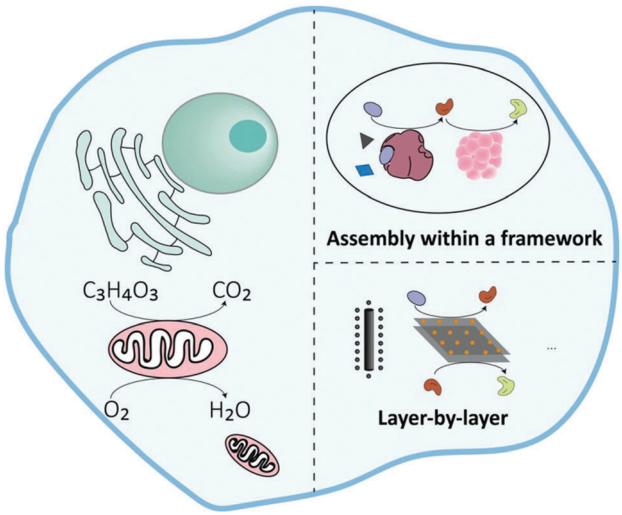

Fig. 1 Schematic illustration of subcellular compartment inspired INAzymes.

2. Synthetic strategies

Inspired by biological systems confining multiple enzymes within subcellular compartments, the INAzymes are usually synthesized with the help of a framework to host two or more nanozymes/enzymes. According to the types of frameworks used, the synthetic strategies of INAzymes are categorized as follows.

2.1 INAzymes based on metal–organic frameworks

Metal–organic frameworks (MOFs), a class of supporting matrix, were first demonstrated by our group to develop INAzymes through co-assembling enzymes and nanozymes.[52] To integrate enzymes with nanozymes, a compatible porous framework must be chosen to tolerate the different reaction conditions. Due to its biocompatible synthesis, good crystallinity, and high surface-area-to-volume ratio, the zeolitic imidazolate framework (ZIF-8) was chosen as a MOF host for the nanoscaled cascade reaction. Through adding GOx and hemin during the self-assembly of Zn^{2+} and 2-methylimidazole, GOx and hemin were encapsulated into ZIF-8 simultaneously, as shown in Fig. 2A. The element mapping of Fe and fluorescence labelling of GOx were performed to validate the successful encapsulation of both hemin and GOx within ZIF-8 (Fig. 2B). Later, catalytic activity studies of the INAzyme and a mixture of separated GOx & hemin demonstrated that such confinement of cascade catalysts within a nanoscale space promoted the catalytic efficiency by 600% compared to that of the mixture of hemin@ZIF-8 and GOx@ZIF-8 (Fig. 2D). This enhancement arose from the confinement of multiple catalysts in the MOFs, which provided a high local concentration of enzymes

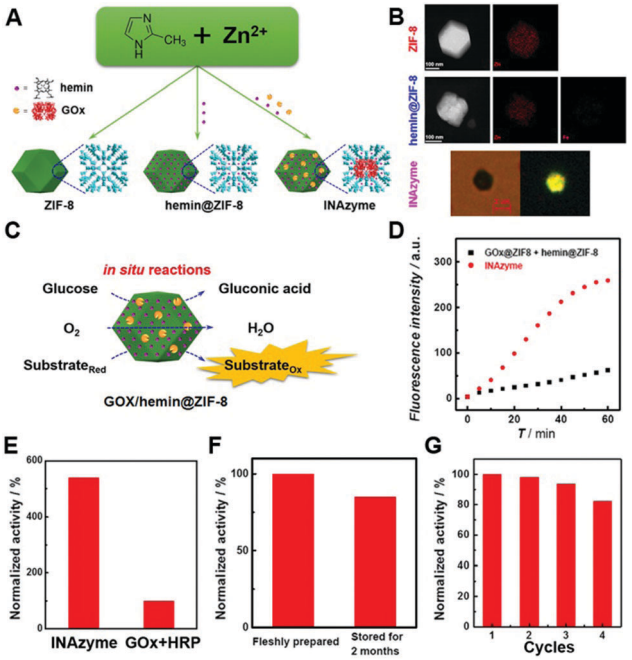

Fig. 2 (A) Schematic illustration of the ZIF-8 modelled INAzyme. (B) TEM images and the corresponding element mapping for ZIF-8 and hemin@ZIF-8, as well as bright field and the corresponding fluorescence images of GOx-FITC/hemin@ZIF-8 (λ_{ex} = 436 nm; FITC, fluorescein isothiocyanate isomer I). (C) Schematic illustration of reactions catalyzed by the INAzymes. (D) Kinetic plots of time-dependent fluorescence intensity of the INAzyme or the mixture of hemin@ZIF-8 and GOx@ZIF-8. (E) Normalized catalytic activities of the INAzyme and free GOx + HRP evaluated after 80 °C treatment. (F) Normalized cascade enzymatic activity of freshly prepared and 2 month-old INAzymes. (G) Normalized catalytic activities of the INAzyme after recycling. (Adapted with permission from ref. 52. Copyright (2016) American Chemical Society.)

and substrates, reduced the barrier of mass transfer, and minimized the decomposition of H_2O_2. Additionally, the ZIF-8 framework protected the encapsulated enzymes from thermal denaturation. As shown in Fig. 2E, the INAzyme exhibited 500% higher activity than that of free GOx + HRP (horseradish peroxidase) after heat treatment. Good long-term storage stability of the INAzyme was also demonstrated as 85% activity was retained after 2 months' storage at 4 °C (Fig. 2F). In addition, such integration not only simplified the recycling process of the INAzyme but still retained 80% activity after four recycles (Fig. 2G).

Notably, this strategy was applicable to other enzymes[52] (*i.e.*, LOx/hemin@ZIF-8, LOx for lactate oxidase), nanozymes[53] (*i.e.*, GOx/NiPd@ZIF-8), and even three more biocatalysts[52] (*i.e.*, invertase/GOx/hemin@ZIF-8), all of which showed enhanced catalytic activities and improved stability. As shown in Fig. 3A and C,

Table 1 Comparison of properties of INAzymes[a]

	Cost	Thermal stability	Long-term stability	Recycle	Toxicology
Enzyme + nanozyme	Medium	Low–medium	Months	Several times	Depending on framework
Nanozyme + nanozyme	Low	High	Months	Several times	Depending on nanozyme
Enzyme + enzyme	High	Low	Days	Few times	Biocompatible

[a] For comparison, "enzyme + enzyme" encapsulated within a framework is also listed.

 This journal is © The Royal Society of Chemistry 2018

Published on 13 March 2018. Downloaded by NANJING UNIVERSITY on 22/04/2018 09:59:00.

LOx was co-assembled with hemin inside ZIF-8 to form a LOx/hemin@ZIF-8 INAzyme. Nearly 400% enhancement in the catalytic activity of LOx/hemin@ZIF-8 was observed compared with the mixture of LOx@ZIF-8 and hemin@ZIF-8. LOx/hemin@ZIF-8 also exhibited remarkable thermal stability relative to free LOx + HRP. Moreover, if another biocatalyst (such as invertase) was added, a triple INAzyme of invertase/GOx/hemin@ZIF-8 could be constructed as well. Such a confinement of cascade catalysts within the nano-scaled space would not only significantly improve the catalysts' stability but also effectively promote the sequential reactions with a 700% enhancement compared to that of the mixture of separated invertase@ZIF-8, GOx@ZIF-8, and hemin@ZIF-8 (Fig. 3B and D). Similarly, other nanozymes could also be encapsulated together with a natural enzyme into ZIF-8 to prepare high-performance INAzymes.[53,54] For example, Dong *et al.* used NiPd instead of hemin as a peroxidase mimic and found that the hollow NiPd nanostructure would help capture more GOx molecules into ZIF-8. Therefore, the catalytic activity enhancement of the GOx/NiPd@ZIF-8 was attributed to the high local concentration of GOx.[53]

Besides ZIF-8, other MOFs with porous and thermally stable structures were also used as the frameworks to construct INAzymes. For example, we developed the peroxidase-mimicking nanozyme AuNPs@MIL-101 by *in situ* reducing a gold precursor within MIL-101 and then assembled natural enzymes onto the AuNPs@MIL-101 to obtain INAzymes (Fig. 4A).[55] The assembled oxidase

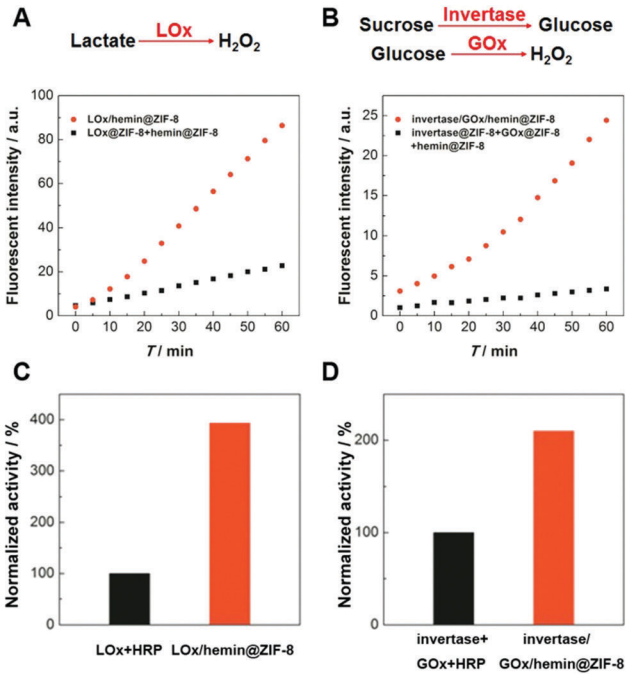

Fig. 3 (A) Kinetic plots of time-dependent fluorescence intensity of the LOx/hemin@ZIF-8 INAzyme or the mixture of hemin@ZIF-8 and LOx@ZIF-8. (B) Kinetic plots of time-dependent fluorescence intensity of the invertase/GOx/hemin@ZIF-8 INAzyme or the mixture of invertase@ZIF-8, GOx@ZIF-8, and hemin@ZIF-8. (C) Normalized catalytic activities of the LOx/hemin@ZIF-8 INAzyme and free LOx + HRP evaluated after 80 °C treatment. (D) Normalized catalytic activities of the invertase/GOx/hemin@ZIF-8 INAzyme and free invertase + GOx + HRP evaluated after 80 °C treatment. (Adapted with permission from ref. 52. Copyright (2016) American Chemical Society.)

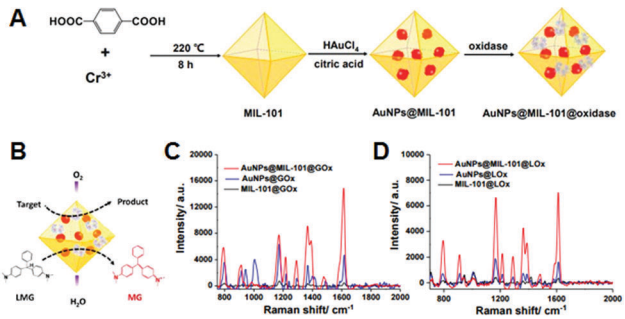

Fig. 4 (A) Schematic illustration of the MIL-101 modelled INAzyme. (B) Schematic illustration of cascade reactions with the corresponding INAzyme. (C) SERS spectra of AuNPs@GOx + glucose, MIL-101@GOx + glucose, and AuNPs@MIL-101@GOx + glucose, respectively. (D) SERS spectra of AuNPs@LOx + lactate, MIL-101@LOx + lactate, and AuNPs@MIL-101@LOx + lactate, respectively. (Adapted with permission from ref. 55. Copyright (2017) American Chemical Society.)

oxidized the substrate (*i.e.*, glucose or lactate) to produce H_2O_2, which would continue to oxidize leucomalachite green (LMG) into Raman-active malachite green (MG) *via* the AuNPs' catalysis, with surface-enhanced Raman scattering (SERS) signals generated for measurements (Fig. 4B). As expected, the cascade catalytic activities were distinguishable from that of AuNPs@GOx or AuNPs@LOx, owing to the improved stability and promoted cascade efficacy of the INAzymes (Fig. 4C and D).

Another interesting triple INAzyme of Pt@CuMOFs–hemin/G-quadruplex–GOx was reported by Xu and co-workers.[56] The synthetic method was similar to that of Au@MIL-101@GOx. First, CuMOFs with a large surface area and high stability were selected to *in situ* grow Pt NPs. Then, the Pt@CuMOFs were assembled with a G-rich sequence, hemin, and GOx to form Pt@CuMOFs–hemin/G-quadruplex–GOx. For this triple INAzyme, the significantly enhanced catalytic activity arose not only from the nanoscale proximity effects but also from the synergistic peroxidase-like activities of both Pt@CuMOFs and the hemin/G-quadruplex.

2.2 INAzymes based on mesoporous silica/carbon

In addition to MOFs, mesoporous silica-based nanomaterials, due to their large surface area, high loading capacity, and good biocompatibility, have been widely used as one of the most favorable biocatalyst supports.[57,58] For instance, Shi *et al.* successfully loaded peroxidase-like small Fe_3O_4 and GOx into the around 40 nm large mesopores of dendritic mesoporous silica NPs (DMSNs) to form the Fe_3O_4–GOx@DMSNs INAzyme, as shown in Fig. 5A.[57] Such an integration would inhibit the decomposition of intermediate H_2O_2 and result in efficient tumor-cell apoptosis. More details about the use of the INAzyme for tumor therapy are discussed in Section 3.3.

Several studies have also used mesoporous carbon as a framework to synthesize INAzymes.[59–61] First, a carbon precursor and iron source were loaded into the mesopores of a silica foam template. Then, thermal treatment and silica removal resulted in magnetic mesoporous carbon. Finally, GOx was assembled into the magnetic mesocellular carbon to obtain the final nanocomposite

Published on 13 March 2018. Downloaded by NANJING UNIVERSITY on 22/04/2018 09:59:00.

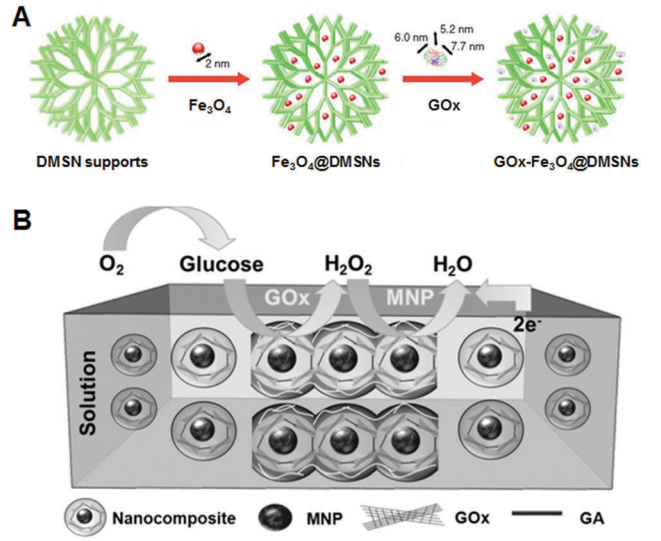

Fig. 5 (A) Synthetic procedure for Fe_3O_4@DMSNs and GOx–Fe_3O_4@DMSNs. (Adapted with permission from ref. 57. Copyright (2017) Nature Publishing Group.) (B) Schematic illustration of the nanocomposite entrapping both magnetic nanoparticles (MNPs) and GOx in mesoporous carbon. (Reprinted with permission from ref. 59. Copyright (2011) John Wiley and Sons.)

(Fig. 5B). This INAzyme exhibited excellent long-term stability as over 90% of the initial catalytic activity was retained after 2 months of storage at room temperature.[59]

In another study, Qu *et al.* integrated AuNPs (GOx mimic) and hemin (peroxidase mimic) into a graphene–mesoporous silica hybrid (GS) to construct the GS–hemin–AuNPs nanohybrid (GSHA) INAzyme (Fig. 6A).[62] This GS allowed the controlled spatial assembly of AuNPs and hemin. Due to the π–π stacking, the hemin would adsorb on the exposed graphene surface to form GS–hemin (GSH). Later, AuNPs grew on the silica surface *via* the electronic interaction between gold and the NH_2 group. Such an integration made the mass transfer efficient and inhibited the decomposition of H_2O_2, thus more than 200% 3,3,5,5-tetramethylbenzidine (TMB) was oxidized by GSHA compared with the mixture of GSH + GS–AuNPs (GSA) (Fig. 6B and C). While for the GS–AuNPs–hemin nanohybrids (GSAH), which grew AuNPs before hemin adsorption, lower catalytic activity was observed due to the inhibition of the GOx-like activity of the AuNPs by hemin. Furthermore, they used a permeable membrane to coat the mesoporous silica nanoparticle (MSN)–AuNPs before hemin adsorption. The obtained MSN–AuNPs–hemin INAzyme improved the catalytic activity by 150% compared to that of the mixture of MSN–AuNPs and MSN–hemin.[63] However, it should be noted that the activity of the INAzyme is still lower than that of the natural enzyme coupled system (Fig. 6C). Thus, the development of new INAzymes with high activity and substrate specificity remains a goal, which we will discuss in the Conclusions and perspectives section.

2.3 INAzymes based on hydrogels

An interesting strategy for encapsulating the nanozymes into an *in situ* formed framework was reported by Wang and co-workers.[64] As shown in Fig. 7, with the addition of glucose

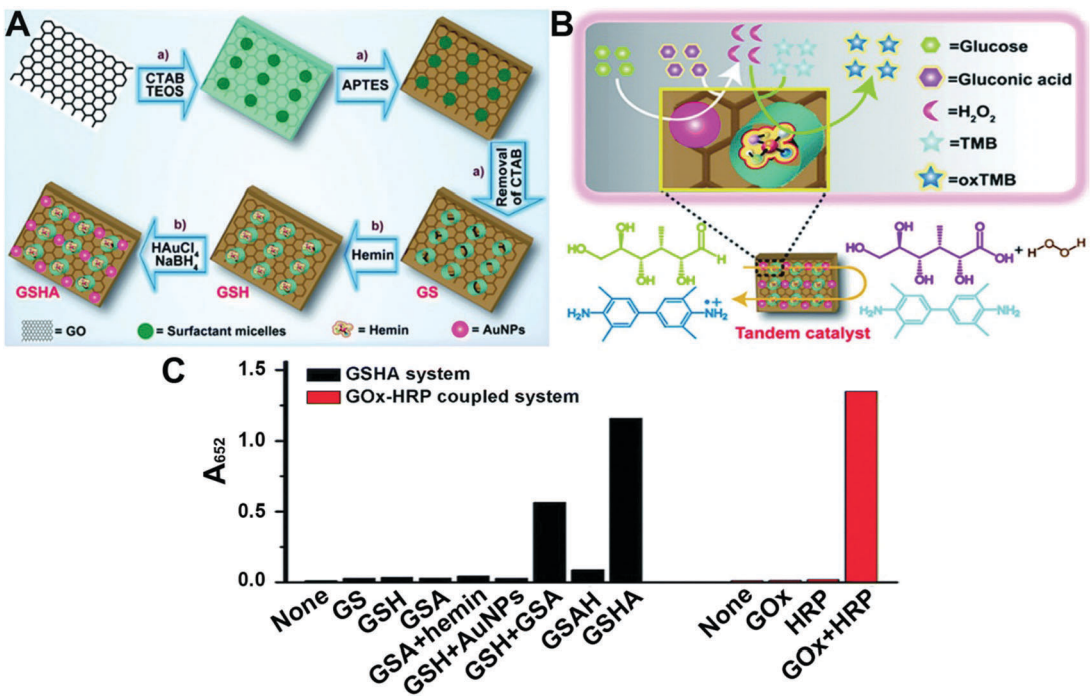

Fig. 6 (A) Synthetic strategy for the construction of the GS–hemin–AuNP nanohybrid (GSHA) catalyst. (B) Schematic illustration of a two-step reaction taking place in the GSHA system. (C) Comparison of TMB oxidation catalyzed by the GSHA system and the GOx–HRP coupled enzyme system in phosphate buffer (0.5 mM, pH 7.0), ([TMB] = 1 mM, [GS, GSA, GSH, GSAH, GSHA] = 1 mg mL^{-1}, [glucose] = 200 mM for the artificial enzyme or 4 mM for the natural enzyme, [GOx] = 100 μg mL^{-1}, [HRP] = 1 ng mL^{-1}). (Adapted with permission from ref. 62. Copyright (2015) Royal Society of Chemistry.)

This journal is © The Royal Society of Chemistry 2018

Published on 13 March 2018. Downloaded by NANJING UNIVERSITY on 22/04/2018 09:59:00.

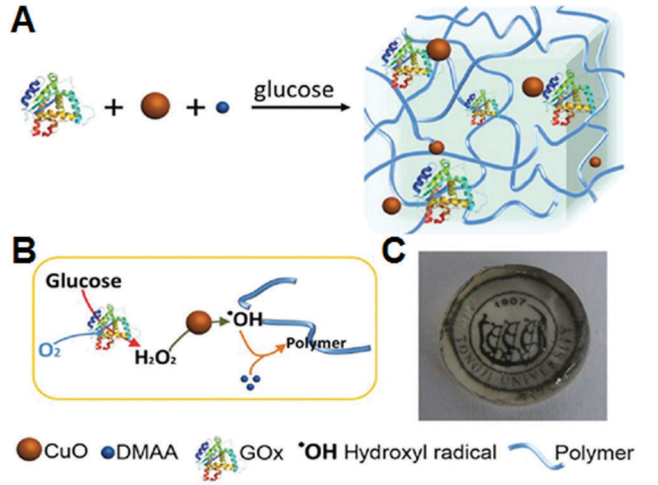

Fig. 7 Nanozyme–gel formation and initiation mechanism. (A) Formation of nanozyme–gel. (B) Initiation mechanism of the nanozyme–gel. (C) Nanozyme–gel on the top of a printed logo. (Reprinted with permission from ref. 64. Copyright (2017) Royal Society of Chemistry.)

to a mixture of GOx, CuO, and the monomer *N*,*N*-dimethylacrylamide, hydroxyl radicals (•OH) would be generated by decomposing H_2O_2. The •OH triggered the mild polymerization of the monomer to form a nanozyme–gel INAzyme system under physiological conditions. By changing the GOx/glucose to H_2O_2, the nanozyme–gel could not be obtained. This is because more oxygen in this system would generate peroxyl radicals rather than hydroxyl radicals, and the former inhibited the monomer polymerization.

2.4 INAzymes *via* a layer-by-layer strategy

Unlike the above-mentioned synthetic strategies, an additional host is not necessary when developing INAzymes through a layer-by-layer strategy. Hence, multi-dimensional nanostructures could be fabricated to realize localized tandem reactions, as shown in Fig. 8. Qu and co-workers used poly-dopamine (PDA) to link V_2O_5 nanowires (serving as glutathione peroxidase (GPx) mimic) and AuNPs (GOx mimic)[65] or MnO_2 NPs (acting as superoxide dismutase (SOD) and catalase mimics).[66] Therefore, a multifunctional INAzyme was obtained (Fig. 8A). Similarly, Fe_3O_4 capped by different surfactants could immobilize GOx through the strong hydrophobic interaction[67] or electrostatic attraction[68,69] between capping agents and GOx to form Fe_3O_4/GOx INAzymes.

In addition, by directly depositing oxidase-like AuNPs into peroxidase-like 2D MOFs, AuNPs/Cu–TCPP(M) INAzymes (TCPP, tetra(4-carboxyphenyl)porphine; M = Fe, Co) were produced, which were then used for *in vitro* glucose detection (Fig. 8B).[70] It should be noted that the 2D MOFs used here were peroxidase mimics, while the MOFs (*i.e.*, ZIF-8 and MIL-101) chosen in the former INAzymes only served as a support without any catalytic activities.

Likewise, the direct growth of AuNPs onto the surface of Fe_3O_4 led to Fe_3O_4–AuNPs INAzymes with both GOx- and peroxidase-like activities. Furthermore, to engineer the dispersibility and stability

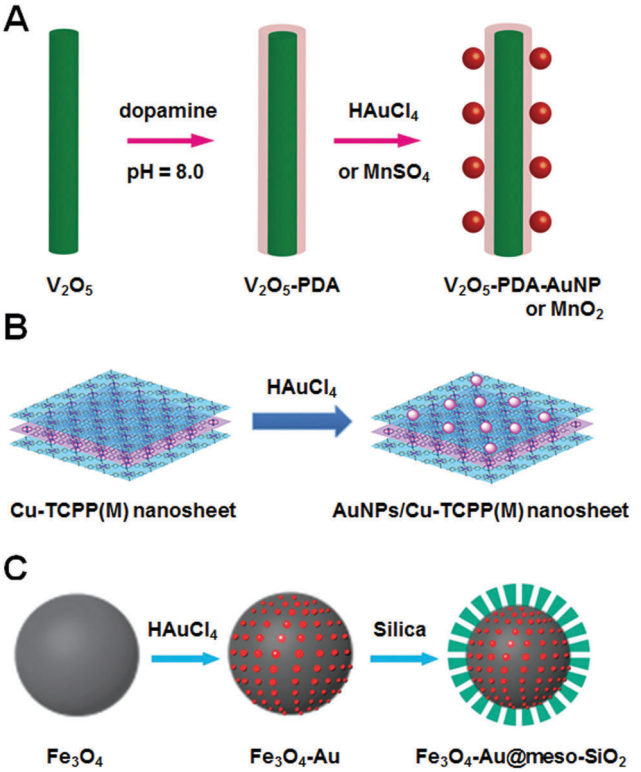

Fig. 8 (A) Schematic illustration of the synthesis of V_2O_5–PDA–AuNPs or MnO_2 nanocomposites. (Adapted with permission from ref. 65 and 66. Copyright (2014 and 2016) John Wiley and Sons.) (B) Schematic illustration of the synthesis of AuNPs/Cu–TCPP(M) hybrid nanosheets (TCPP, tetra-(4-carboxyphenyl)porphine; M = Fe, Co). (Adapted with permission from ref. 70. Copyright (2017) John Wiley and Sons.) (C) Schematic illustration of the synthesis of Fe_3O_4–Au@meso-SiO_2 microspheres. (Reprinted with permission from ref. 71. Copyright (2013) Royal Society of Chemistry.)

of the INAzymes, a mesoporous SiO_2 (meso-SiO_2) layer was introduced onto the surface of the Fe_3O_4–AuNPs, as shown in Fig. 8C.[71] The catalytic activity of the Fe_3O_4–Au@meso-SiO_2 exhibited 300% enhancement compared to that of the mixture of Fe_3O_4 and AuNPs. With the protection of meso-SiO_2, more than 95% activity and the intact structure of Fe_3O_4–Au@meso-SiO_2 microspheres can be maintained after 6 cycles of reaction. While for the mixture of Fe_3O_4 and AuNPs, serious aggregation of the nanoparticles after only one cycle decreased the catalytic activity by more than 50%.

3. Applications of INAzymes

3.1 INAzymes for *in vitro* sensing

Benefiting from the nanoscale proximity effect in Fig. 2C, INAzymes perfectly suit the tandem sensing strategy where the products catalyzed by the first reaction would be consumed instantly as reactants of the second reaction to produce the signalling products. As a result, glucose, lactate, and cholesterol could be detected *in vitro* by integrating GOx/GOx-like AuNPs/LOx/cholesterol oxidase with peroxidase-like nanozymes (Table 2). High specificity and efficiency were obtained with these INAzymes. For example, the V_2O_5–PDA–AuNP INAzyme displayed good sensitivity and selectivity towards glucose detection, with a detection limit of

Published on 13 March 2018. Downloaded by NANJING UNIVERSITY on 22/04/2018 09:59:00.

Table 2 *In vitro* sensing based on INAzymes

INAzymes	Target	Method	Linear range	Detection limit	Comments	Ref.
GOx@hemin@ZIF-8	Glucose	Colorimetric	0–250 μM	1.7 μM	Substrate: 2,2′-azino-bis(3-ethylbenzothiazoline-6-sulphonic acid) (ABTS) Selectivity against: acrobatic acid, lactate, dopamine, 3,4-dihydroxyphenylacetic acid, uric acid, and 5-hydroxytryptamine.	52
GOx/NiPd@ZIF-8	Glucose	Colorimetric & electrochemical	10–300 μM & 0.1–1.7 mM	9.2 μM	Substrate: *o*-phenylenediamine Selectivity against: fructose, maltose, lactose, and sucrose	53
GOx/Fe_3O_4@ZIF-8	Glucose	Colorimetric	5–150 μM	1.9 μM	Substrate: *o*-phenylenediamine Selectivity against: sodium chloride, calcium chloride, potassium nitrate, fructose, mannose, galactose, and bovine serum albumin	54
AuNPs@MIL-101@GOx	Glucose	Raman	10–200 μM	4.2 μM	Substrate: leucomalachite green Selectivity against: acrobatic acid, dopamine, 3,4-dihydroxyphenylacetic acid, uric acid, and 5-hydroxytryptamine.	55
Fe_3O_4/GOx/mesoporous silica	Glucose	Colorimetric	30–1000 μM	3 μM	Substrate: TMB Selectivity against: lactose, arabinose, galactose, and fructose	58
MNP/GOx/mesoporous carbon	Glucose	Electrochemical	0.5–10 mM	0.2 mM	The composite was used to construct a carbon paste electrode.	59
Casein-Fe_3O_4/GOx composite	Glucose	Colorimetric	3–1000 μM	1 μM	Substrate: TMB Selectivity against: fructose, lactose, and maltose	67
Poly(diallyldimethylammonium chloride)–GOx–Fe_3O_4 composite	Glucose	Colorimetric	30–100 μM & 0.2–1 mM	30 μM	Substrate: ABTS Selectivity against: arabinose, cellobiose, galactose, lactose, maltose, raffinose, and xylose.	68
Poly(diallyldimethylammonium chloride)–GOx–Fe_3O_4 composite	Glucose	Fluorometric	3–9 μM & 20–100 μM	3 μM	Substrate: amplex ultrared Selectivity against: arabinose, cellobiose, galactose, lactose, maltose, raffinose, and xylose.	69
GOx/Fe_3O_4@Fe^{3+}/adenosine 5′-monophosphate coordination polymers	Glucose	Colorimetric	0–100 μM	1.4 μM	Substrate: ABTS Selectivity against: fructose, galatose, sucrose, sodium chloride, and albumin	72
GOx/Fe_3O_4/graphene oxide nanocomposite	Glucose	Colorimetric	0.5–600 μM	0.2 μM	Substrate: *N*,*N*-diethyl-*p*-phenylenediamine sulphate Selectivity against: K^+, CO_3^{2-}, SO_4^{2-}, NO_3^-, Cl^-; Mg^{2+}, Zn^{2+}, Ca^{2+}; Al^{3+}, Ba^{2+}, L-phenylalanine, glycine, arginine; EDTA; Cu^{2+}; Fe^{3+}; bilirubin; hemoglobin, ascorbic acid	73
AuNPs/Cu–TCPP(M) (M = Fe, Co)	Glucose	Colorimetric	10–300 μM	8.5 μM	Substrate: TMB	70
Fe_3O_4–Au@meso-SiO_2 microspheres	Glucose	Colorimetric	10–130 μM	0.5 μM	Substrate: TMB	71
V_2O_5–PDA–AuNP	Glucose	Colorimetric	0–10 μM	0.5 μM	Substrate: ABTS Selectivity against: fructose, lactose, and maltose	65
AuNPs@MIL-101@LOx	Lactate	Raman	10–200 μM	5.0 μM	Substrate: leucomalachite green Selectivity against: acrobatic acid, dopamine, 3,4-dihydroxyphenylacetic acid, uric acid, and 5-hydroxytryptamine.	55
Fe_3O_4/cholesterol oxidase/mesoporous silica	Cholesterol	Colorimetric	10–250 μM	5 μM	Substrate: TMB Selectivity against: glycerol, and glucose	58
Poly(diallyldimethylammonium chloride)–galactose oxidase–Fe_3O_4 composite	Galactose	Fluorometric	2–80 μM	2 μM	Substrate: amplex ultrared	69
Poly(diallyldimethylammonium chloride)–choline oxidase–Fe_3O_4 composite	Choline	Fluorometric	20–100 μM	20 μM	Substrate: amplex ultrared	69
V_2O_5–PDA–AuNP	Single-stranded DNA	Colorimetric	0–0.1 μM	2.3 nM	Substrate: ABTS	65
Pt@CuMOFs–hemin/G-quadruplex–GOx	Carcinoembryonic antigen (CEA)	Electrochemical	0.05–20 ng mL^{-1}	0.023 pg mL^{-1}	Substrate: 3,3-diaminobenzidine Selectivity against: thrombin, human immunoglobulin G, alpha-fetoprotein, and prostate-specific antigen	56

This journal is © The Royal Society of Chemistry 2018

Published on 13 March 2018. Downloaded by NANJING UNIVERSITY on 22/04/2018 09:59:00.

as low as 0.5 μM.[65] In addition by taking advantage of the different affinities of single-stranded DNA and double-stranded DNA towards AuNPs, the GOx-like activity of AuNPs would be suppressed to a different extent. Therefore, colorimetric sensing of target DNA was achieved with the V_2O_5–PDA–AuNP INAzymes.[65]

An innovative concept for an electrochemical impedimetric aptasensor for carcinoembryonic antigen (CEA) was reported by using the Pt@CuMOFs–hemin/G-quadruplex–GOx triple INAzyme.[56] The CEA aptamers (Apt1 and Apt2) were immobilized onto an AuNP-modified electrode and the triple INAzyme, respectively. In the presence of the target CEA, a sandwich-type assay was fabricated with INAzymes captured onto the electrode surface, and then nonconductive insoluble precipitates would form to give the impedimetric signal. With the developed electrochemical impedimetric aptasensor, the response signal was efficiently amplified by the enhanced catalytic activities of the INAzyme. As low as 0.023 pg mL^{-1} of target CEA was detected, which made clinical detection promising.

3.2 INAzymes for *in vivo* sensing

As mentioned above, the promoted activity and enhanced stability of INAzymes offered the possibility of functioning under complex physiological conditions. Recently, we have engineered an INAzyme for *in vivo* neurochemical monitoring in living brains.[52,55] First, the dynamic linear range from 0 to 250 μM obtained from *in vitro* sensing enabled the further measurements of cerebral glucose in living brains, as this range covered the physiological levels of microdialyzed glucose. Then, an off-line detection of glucose in living brains was developed with the help of *in vivo* microdialysis (Fig. 9A). Through mixing the microdialyzed samples with the INAzyme and substrates, the products catalysed by cascade reactions would be generated for signalling. For the GOx@hemin@ZIF-8 INAzyme, both 2,2′-azino-bis(3-ethylbenzothiazoline-6-sulphonic acid) and Ampliflu Red were used for producing green-colored and fluorescent signals, respectively. However by using AuNPs@MIL-101@GOx, Raman spectra of malachite green would be produced for signalling. Both INAzyme systems showed a decreased glucose level after global cerebral ischemia, as the blockage of cerebral blood flow resulted in an enhanced metabolism consumption.

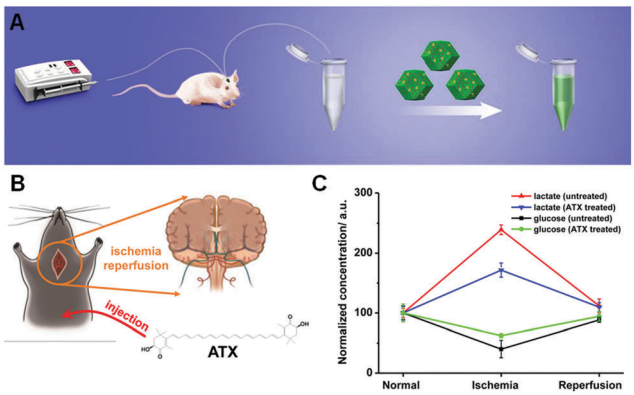

Fig. 9 (A) Schematic illustration of off-line measurement of glucose in the brain of living rats *via* INAzyme-catalyzed cascade reactions. (Reprinted with permission from ref. 52. Copyright (2016) American Chemical Society.) (B) Schematic illustration of global cerebral ischemia/reperfusion and the treatment with ATX. (C) Dynamic changes of glucose and lactate following ischemia and reperfusion with and without ATX pretreatment. The glucose and lactate levels before ischemia were normalized as 100. (Reprinted with permission from ref. 55. Copyright (2017) American Chemical Society.)

Furthermore, the SERS active INAzyme was applied for evaluating the therapeutic effects of potential drugs like astaxanthin (ATX).[55] If ischemic stroke occurred, the striatum glucose level would decrease while the lactate level would increase. When an anti-oxidation drug like ATX was used for treatment, both the glucose and lactate fluctuation level should be suppressed. Fig. 9B and C demonstrate that ATX could be an effective drug for alleviating cerebral ischemic injuries. In addition to monitoring glucose and lactate in living brains and evaluating the therapeutic effects, this effective bioassay based on a SERS INAzyme could also discriminate abnormal metabolism in tumors from that in normal tissues. Concentrations of 83.3 ± 4.7 and 16.1 ± 4.1 μM were measured for glucose and lactate in normal tissues. Attributed to the Warburg effects of tumors, the concentration of glucose decreased as low as to be barely measurable. However the lactate amount displayed was 187.7 ± 98.7 μM, nearly 10 times higher than that of normal tissues.

Though the INAzyme could be used for effective detection of glucose in living rats, the off-line sensor still suffered from a poor temporal resolution, which hence limits future practical applications. To overcome this limitation, we went on to construct an online measurement platform by immobilizing the INAzyme into the channel of a microfluidics chip.[52] When assisted with *in vivo* microdialysis, the dynamic changes of cerebral glucose following global ischemia and perfusion could be successfully monitored with the INAzyme-based analytic platform (Fig. 10A). Due to the fast reaction and strong fluorescence of the oxidized products, Ampliflu Red was chosen to meet the requirements of continuous *in vivo* measurements. As shown in Fig. 10B, the glucose levels decreased to 49.1 ± 12.7% of the basal level after global ischemia, which was consistent with the off-line measured values 50.2 ± 8.3%. Later, the value was restored to 98.4 ± 10.1% of the basal level during the reperfusion process. This prototypical device may aid researchers to explore with profundity the mechanism of an unclear illness by real time monitoring.

Another important aspect of *in vivo* sensing is the biomedical imaging of a cell or organ, which was demonstrated by Shi *et al.*[57] The Fe_3O_4–GOx@DMSNs INAzyme (Fig. 5A) was used to produce harmful hydroxyl radicals *in situ* in cancer cells through the designed cascade reaction. Then, the produced hydroxyl radicals were imaged by using a reactive oxygen species (ROS) fluorescent probe, 2′,7′-dichlorofluorescein diacetate. And a quantitative evaluation of the generated hydroxyl radicals and mapping of the glucose distribution in cancer cells could be achieved through analysing the corresponding fluorescence intensity.

3.3 INAzymes for therapeutics

Nanozymes have been exploited for potential therapeutics *via* eliminating ROS, such as H_2O_2, $^{\bullet}OH$, and $^{\bullet}O_2^{-}$.[2] To provide an

Published on 13 March 2018. Downloaded by NANJING UNIVERSITY on 22/04/2018 09:59:00.

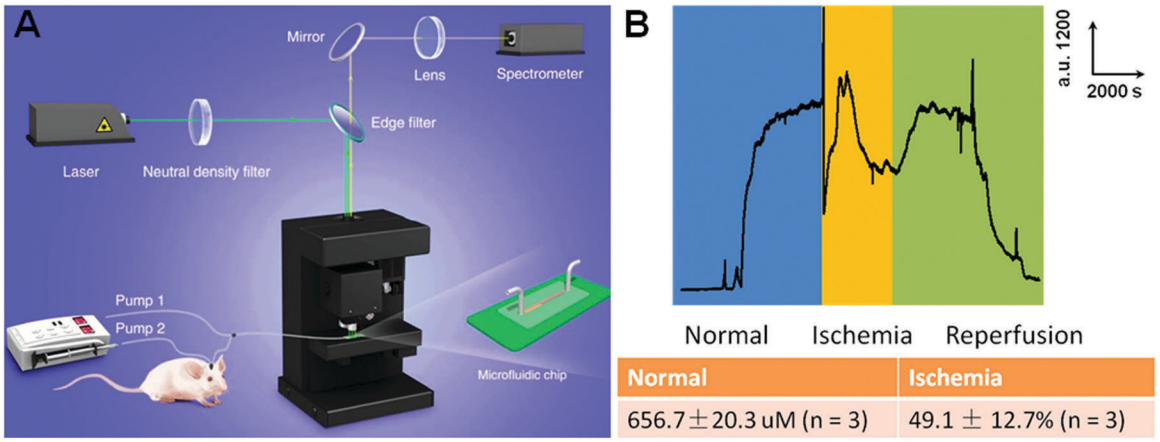

Fig. 10 (A) The INAzyme-based integrative fluorescence sensing platform for continuous *in vivo* measurement of neurochemicals (glucose is an example here) in living rats. The platform mainly consisted of three parts: (a) the microdialysis device, which included two pumps with syringes, a microdialysis probe (inserted in the rat's brain), and a T-junction, connected with tubing; (b) the fluorescence microscope, which included the excitation laser and a spectrometer; and (c) the microfluidic chip, which was connected with the microdialysis device *via* tubing and had the INAzyme immobilized in its microchannel. The 532 nm laser through the microscope was focused onto the sample within the microchannel at a distance of 2 mm from the outlet. The resultant fluorescence spectra of the sample were continuously collected. (B) Continuously monitoring the dynamic change of the glucose level in the striatum of a living rat brain following global ischemia/reperfusion with the INAzyme-based sensing platform. (Adapted with permission from ref. 52. Copyright (2016) American Chemical Society.)

enhanced antioxidative effect, Qu and co-workers developed a V_2O_5–PDA–MnO_2 INAzyme to mimic natural ROS defenders with improved catalytic activity and efficiency.[66] For this INAzyme, MnO_2 NPs served as SOD and catalase mimics while V_2O_5 acted as a GPx mimic, which mimicked the intracellular antioxidant defense process where SOD, CAT, and GPx co-participated. Even PDA was also found to be an efficient antioxidant. Owing to the excellent ROS scavenging abilities of assembled INAzymes, an anti-inflammation model was successfully built (Fig. 11). After the treatment of the V_2O_5–PDA–MnO_2 nanocomposites, the fluorescence intensity of the phorbol 12-myristate 13-acetate (PMA)-treated ear decreased.

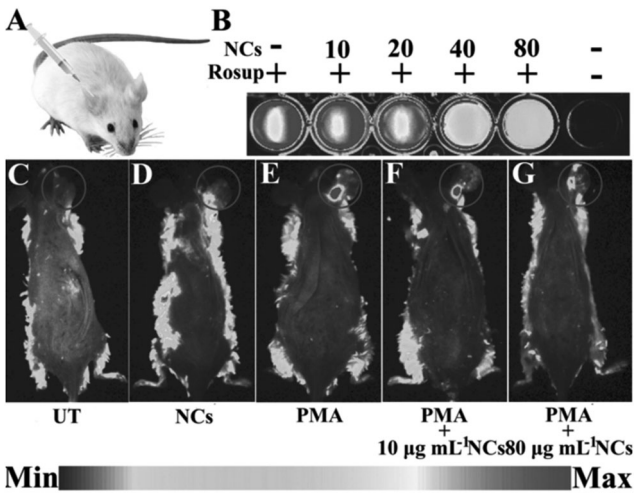

Fig. 11 (A) Scheme of the inflammation model. (B) Luminescence images of various concentrations of V_2O_5–PDA–MnO_2 hybrid nanocomposites in the presence or absence of Rosup using the *in vivo* imaging system. (C)–(G) *In vivo* imaging of the effect of the nanocomposites on ROS scavenging in PMA-induced ear inflammation. (Reprinted with permission from ref. 66. Copyright (2016) John Wiley and Sons.)

In contrast to eliminating ROS for anti-oxidation/anti-inflammatory effects, several studies reported the applications of nanozyme-produced •OH for anti-bacteria or anti-tumor use. For instance, Wang and co-workers fabricated an INAzyme based on a hydrogel system with *in situ* generated •OH for antibacterial effects. The cell wall structure of the bacterial membrane could be destroyed through oxidizing the unsaturated bonds of the phospholipids by •OH.[64]

Recently, Shi *et al.* demonstrated that •OH could do harm to cancer cells.[57] As shown in Fig. 12A, ultrasmall Fe_3O_4 together with natural GOx were encapsulated in dendritic mesoporous silica nanoparticles forming GOx–Fe_3O_4@DMSNs nanocatalysts (GFD NCs). After being taken up by cancer cells, H_2O_2 produced from oxidation of glucose by GOx decomposed into harmful hydroxyl radicals during the catalysis process of Fe_3O_4. Meanwhile, the consumption of glucose would also starve the cancer cells. Hence, therapeutic INAzymes with the ability to kill cancer cells were established.

Before therapy, the *in vivo* biosafety issue and pharmacokinetics of intravenously injected GFD NCs were investigated. Compared with the control group, the administration of GFD NCs did not show any significant effect on the mouse growth and organ functions, indicating the high biocompatibility of such INAzymes. Besides, the effective accumulation in tumors, the increasing distribution kinetics in the whole blood, as well as the 2.65 h circulating half-life all demonstrated the improved pharmacokinetics.

Then, to verify the therapeutics effects, 4T1 mammary tumor xenografts on specific pathogen-free BALB/c nude mice were treated with GFD NCs both intravenously and intratumorally (Fig. 12B). Fig. 12C–H demonstrates that 4T1 mammary tumor

Published on 13 March 2018. Downloaded by NANJING UNIVERSITY on 22/04/2018 09:59:00.

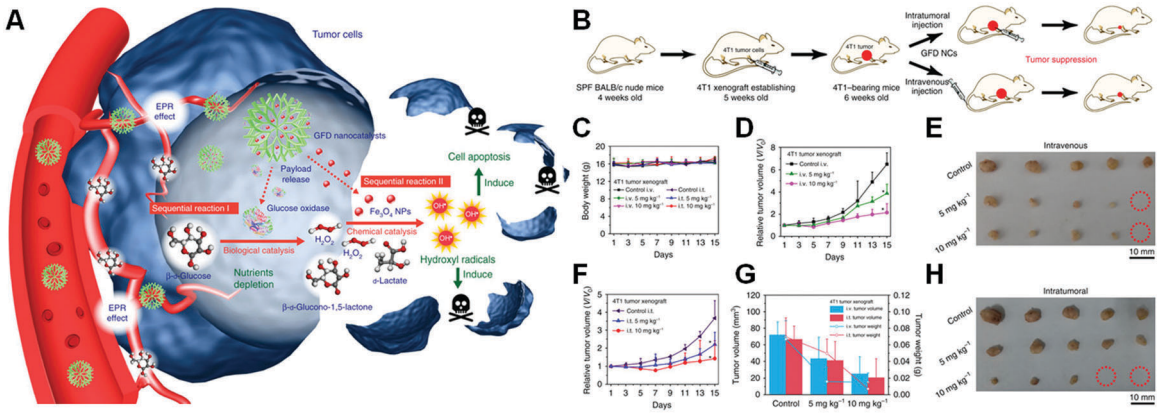

Fig. 12 (A) The scheme of the sequential catalytic-therapeutic mechanism of GFD NCs for the generation of hydroxyl radicals for cancer therapy. (B) Schematic illustration of 4T1 tumor xenograft establishment, saline and GFD NC administration modalities, and therapeutic outcome. (C) The body weights of nude mice bearing 4T1 tumor xenografts after injections with saline (control group) and GFD NCs (5 and 10 mg kg^{-1}, therapeutic group) intravenously and intratumorally, respectively. The relative tumor volumes of 4T1 bearing nude mice treated with saline (control group) and different doses of GFD NCs (therapeutic group) *via* (D) intravenous and (F) intratumoral modes (n = 5). All the above data were collected and measured every 2 days. Statistical significance is assessed by Student's one-sided t test compared with the control group. *$p < 0.05$, **$p < 0.01$. (G) The tumor volumes and tumor weights of dissected tumors from each group after 15 days of therapy. Digital photographs of the dissected tumors from (E) intravenous and (H) intratumoral groups after 15 days of therapy. Red circles indicate the eliminated tumors. (Adapted with permission from ref. 57. Copyright (2017) Nature Publishing Group.)

growth could be effectively suppressed after the administration of GFD NCs both intravenously and intratumorally. With 10 mg kg^{-1} of GFD NCs treated intravenously and intratumorally, the tumor-suppression rates were estimated to be 64.67% and 68.89%, respectively. And the general applications of therapeutics INAzymes were further demonstrated on another tumor xenograft (U87 glioblastoma model), which provided a promising strategy for effective tumor therapy. Besides, the biodegradation studies of GFD NCs indicated that the destruction of the dendritic structures would help the therapeutic INAzyme excrete out of the body finally.

4. Conclusions and perspectives

Nanozymes, as one of the most emerging branches in the field of nanotechnology, though gaining achievable outcomes, still face numerous challenges. Integrating different nanozymes/enzymes as a whole has partially solved the limitations of insufficient activity and poor selectivity. In this Feature Article, synthetic strategies and biomedical applications of INAzymes have been summarized and discussed in detail. Many exciting advancements have been achieved with high-performance INAzymes, including engineering INAzymes for *in vivo* cerebral sensing. However, some critical issues still need to be addressed for the further development of INAzymes.

(a) We speculate that by taking advantage of the multiple enzyme mimicking activities of nanozymes, single component INAzymes could be constructed to realize a cascade reaction.[74] Such all-in-one nanozymes may reveal insights into the ultimate form of INAzymes, but the mechanism of multi-enzyme mimicking nanozymes remains to be investigated.

(b) While the robustness of single component INAzymes may save cost, the specificity is sacrificed without the involvement of natural enzymes. Therefore, the rational construction of protein-like binding pockets[75] or the utilization of molecularly imprinted polymers[76] may be considered in further INAzyme design.

(c) The efficiency and activity of INAzymes was enhanced, but is still lower than those of natural enzymes. As the activity of nanozymes mainly comes from the nanomaterials themselves, high-performance INAzymes could be developed by engineering the physical and chemical properties of nanozymes.

(d) Although some achievements have been made for the *in vivo* biomedical applications of INAzymes, various problems such as clinical toxicity, poor pharmacokinetics profiles, and immunogenicity should be fully investigated to further advance the field. Some preliminary results about the toxicity and pharmacokinetics have been reported, which indicated the potential biocompatibility and good pharmacokinetics of INAzymes.[57] Compared with human recombinant enzymes and enzymes encapsulated/modified with biocompatible and FDA-approved polymers,[77] the INAzymes showed a similar high biocompatibility and better pharmacokinetics. Further immunogenicity should also be exploited.

(e) Currently, the therapeutic studies are mainly focused on cancer. Therapeutics for other diseases could be investigated by modulating the ROS levels with INAzymes. Besides sensing and therapeutics, other interesting applications could be explored. For example, SERS active INAzymes have been applied for evaluating the therapeutic efficacy of the ATX drug for ischemic stroke.[55] Therefore, further drug screening would be possible with the help of INAzymes. Developing INAzyme based biomedical devices could be another interesting direction. Besides the biomedical field, the application of INAzymes should also be explored in the environment, agriculture, and national security fields in future studies.

(f) Still, the types of nanozymes and INAzymes constructed by nanomaterials are mainly focused on redox catalysis.

Published on 13 March 2018. Downloaded by NANJING UNIVERSITY on 22/04/2018 09:59:00.

In a broader sense, it is important to design and prepare new nanozymes and INAzymes for other important biocatalytic reactions, supplementing natural and re-combinant enzymes for practical applications.[78]

Conflicts of interest

There are no conflicts to declare.

Acknowledgements

This work was supported by the National Natural Science Foundation of China (21722503 and 21405081), the Natural Science Foundation of Jiangsu Province (BK20160615), the 973 Program (2015CB659400), the PAPD program, the Shuangchuang Program of Jiangsu Province, Open Funds of the State Key Laboratory of Coordination Chemistry (SKLCC1619 and SKLCC1819), Open Funds of the State Key Laboratory of Analytical Chemistry for Life Science (SKLACLS1704), the China Postdoctoral Science Foundation (2016M590437), and the Thousand Talents Program for Young Researchers. We thank the anonymous reviewers for their insightful comments.

Notes and references

1 L. Gao, J. Zhuang, L. Nie, J. Zhang, Y. Zhang, N. Gu, T. Wang, J. Feng, D. Yang, S. Perrett and X. Yan, *Nat. Nanotechnol.*, 2007, **2**, 577–583.
2 H. Wei and E. Wang, *Chem. Soc. Rev.*, 2013, **42**, 6060–6093.
3 Y. Lin, J. Ren and X. Qu, *Acc. Chem. Res.*, 2014, **47**, 1097–1105.
4 X. Wang, Y. Hu and H. Wei, *Inorg. Chem. Front.*, 2016, **3**, 41–60.
5 S. Li, Y. Huang, J. Liu, E. Wang and H. Wei, *Prog. Biochem. Biophys.*, 2018, **45**, 129–147.
6 N. A. Kotov, *Science*, 2010, **330**, 188–189.
7 G. Y. Tonga, Y. Jeong, B. Duncan, T. Mizuhara, R. Mout, R. Das, S. T. Kim, Y.-C. Yeh, B. Yan, S. Hou and V. M. Rotello, *Nat. Chem.*, 2015, **7**, 597–603.
8 C. P. Liu, T. H. Wu, Y. L. Lin, C. Y. Liu, S. Wang and S. Y. Lin, *Small*, 2016, **12**, 4127–4135.
9 H. Ye, K. Yang, J. Tao, Y. Liu, Q. Zhang, S. Habibi, Z. Nie and X. Xia, *ACS Nano*, 2017, **11**, 2052–2059.
10 Y. Song, X. Xia, X. Wu, P. Wang and L. Qin, *Angew. Chem., Int. Ed.*, 2014, **53**, 12451–12455.
11 Y. Fu, X. Zhao, J. Zhang and W. Li, *J. Phys. Chem. C*, 2014, **118**, 18116–18125.
12 X. Shen, W. Liu, X. Gao, Z. Lu, X. Wu and X. Gao, *J. Am. Chem. Soc.*, 2015, **137**, 15882–15891.
13 G. Fang, W. Li, X. Shen, J. M. Perez-Aguilar, Y. Chong, X. Gao, Z. Chai, C. Chen, C. Ge and R. Zhou, *Nat. Commun.*, 2018, **9**, 129.
14 S. Fan, M. Zhao, L. Ding, H. Li and S. Chen, *Biosens. Bioelectron.*, 2017, **89**, 846–852.
15 J. Liu, L. Meng, Z. Fei, P. J. Dyson, X. Jing and X. Liu, *Biosens. Bioelectron.*, 2017, **90**, 69–74.
16 Y. Zhang, Z. Y. Wang, X. J. Li, L. Wang, M. Yin, L. H. Wang, N. Chen, C. H. Fan and H. Y. Song, *Adv. Mater.*, 2016, **28**, 1387–1393.
17 A. A. Vernekar, D. Sinha, S. Srivastava, P. U. Paramasivam, P. D'Silva and G. Mugesh, *Nat. Commun.*, 2014, **5**, 5301.
18 J. Yao, Y. Cheng, M. Zhou, S. Zhao, S. Lin, X. Wang, J. Wu, S. Li and H. Wei, *Chem. Sci.*, 2018, **9**, 2927–2933.
19 M. M. Behrens, S. S. Ali, D. N. Dao, J. Lucero, G. Shekhtman, K. L. Quick and L. L. Dugan, *Science*, 2007, **318**, 1645–1647.
20 L. L. Dugan, L. Tian, K. L. Quick, J. I. Hardt, M. Karimi, C. Brown, S. Loftin, H. Flores, S. M. Moerlein, J. Polich, S. D. Tabbal, J. W. Mink and J. S. Perlmutter, *Ann. Neurol.*, 2014, **76**, 393–402.
21 T. Xue, B. Peng, M. Xue, X. Zhong, C.-Y. Chiu, S. Yang, Y. Qu, L. Ruan, S. Jiang, S. Dubin, R. B. Kaner, J. I. Zink, M. E. Meyerhoff, X. Duan and Y. Huang, *Nat. Commun.*, 2014, **5**, 3200.
22 E. L. G. Samuel, D. C. Marcano, V. Berka, B. R. Bitner, G. Wu, A. Potter, R. H. Fabian, R. G. Pautler, T. A. Kent, A.-L. Tsai and J. M. Tour, *Proc. Natl. Acad. Sci. U. S. A.*, 2015, **112**, 2343–2348.
23 W. Zhang, S. Hu, J. J. Yin, W. He, W. Lu, M. Ma, N. Gu and Y. Zhang, *J. Am. Chem. Soc.*, 2016, **138**, 5860–5865.
24 X. Wang, W. Guo, Y. Hu, J. Wu and H. Wei, *Nanozymes: Next Wave of Artificial Enzymes*, Springer, 2016.
25 F. Manea, F. B. Houillon, L. Pasquato and P. Scrimin, *Angew. Chem., Int. Ed.*, 2004, **43**, 6165–6169.
26 S. Neri, S. Garcia Martin, C. Pezzato and L. J. Prins, *J. Am. Chem. Soc.*, 2017, **139**, 1794–1797.
27 B. E. R. Snyder, P. Vanelderen, M. L. Bols, S. D. Hallaert, L. H. Böttger, L. Ungur, K. Pierloot, R. A. Schoonheydt, B. F. Sels and E. I. Solomon, *Nature*, 2016, **536**, 317–321.
28 R. Cai, D. Yang, S. Peng, X. Chen, Y. Huang, Y. Liu, W. Hou, S. Yang, Z. Liu and W. Tan, *J. Am. Chem. Soc.*, 2015, **137**, 13957–13963.
29 H. Wei and E. Wang, *Anal. Chem.*, 2008, **80**, 2250–2254.
30 M. C. Kim, D. Lee, S. H. Jeong, S. Y. Lee and E. Kang, *ACS Appl. Mater. Interfaces*, 2016, **8**, 34317–34326.
31 V. Sharma and S. M. Mobin, *Sens. Actuators, B*, 2017, **240**, 338–348.
32 X. Wang, W. Cao, L. Qin, T. Lin, W. Chen, S. Lin, J. Yao, X. Zhao, M. Zhou, C. Hang and H. Wei, *Theranostics*, 2017, **7**, 2277–2286.
33 H. Cheng, Y. Liu, Y. Hu, Y. Ding, S. Lin, W. Cao, Q. Wang, J. Wu, F. Muhammad, X. Zhao, D. Zhao, Z. Li, H. Xing and H. Wei, *Anal. Chem.*, 2017, **89**, 11552–11559.
34 H. Cheng, S. Lin, F. Muhammad, Y.-W. Lin and H. Wei, *ACS Sens.*, 2016, **1**, 1336–1343.
35 S. Lin, J. Wu, J. Yao, W. Cao, F. Muhammad and H. Wei, *Nanozymes for Biomedical Sensing Applications: from in vitro Sensing to Living Systems*, Elsevier, 2018.
36 V. Petkov, B. N. Wanjala, R. Loukrakpam, J. Luo, L. Yang, C.-J. Zhong and S. Shastri, *Nano Lett.*, 2012, **12**, 4289–4299.
37 M. Kluenker, M. Nawaz Tahir, R. Ragg, K. Korschelt, P. Simon, T. E. Gorelik, B. Barton, S. I. Shylin, M. Panthöfer, J. Herzberger, H. Frey, V. Ksenofontov, A. Möller, U. Kolb, J. Grin and W. Tremel, *Chem. Mater.*, 2017, **29**, 1134–1146.
38 T. Kito, R. Shibata, M. Ishii, H. Suzuki, T. Himeno, Y. Kataoka, Y. Yamamura, T. Yamamoto, N. Nishio, S. Ito, Y. Numaguchi, T. Tanigawa, J. K. Yamashita, N. Ouchi, H. Honda, K. Isobe and T. Murohara, *Sci. Rep.*, 2013, **3**, 1418.
39 J. Chen, S. Patil, S. Seal and J. F. McGinnis, *Nat. Nanotechnol.*, 2006, **1**, 142–150.
40 M. Saeed and L. Deng, *Int. J. Greenhouse Gas Control*, 2016, **53**, 254–262.
41 F. Natalio, R. André, A. F. Hartog, B. Stoll, K. P. Jochum, R. Wever and W. Tremel, *Nat. Nanotechnol.*, 2012, **7**, 530–535.
42 L. Wan, J. Liu and X.-J. Huang, *Chem. Commun.*, 2014, **50**, 13589–13591.
43 Y. Jv, B. Li and R. Cao, *Chem. Commun.*, 2010, **46**, 8017–8019.
44 J. Wang, D. Han, X. Wang, B. Qi and M. Zhao, *Biosens. Bioelectron.*, 2012, **36**, 18–21.
45 Y.-L. Dong, H.-G. Zhang, Z. U. Rahman, L. Su, X.-J. Chen, J. Hu and X.-G. Chen, *Nanoscale*, 2012, **4**, 3969–3976.
46 H. Liang, S. Jiang, Q. Yuan, G. Li, F. Wang, Z. Zhang and J. Liu, *Nanoscale*, 2016, **8**, 6071–6078.
47 Z. Zhao, J. Fu, S. Dhakal, A. Johnson-Buck, M. Liu, T. Zhang, N. W. Woodbury, Y. Liu, N. G. Walter and H. Yan, *Nat. Commun.*, 2016, **7**, 10619.
48 O. I. Wilner, Y. Weizmann, R. Gill, O. Lioubashevski, R. Freeman and I. Willner, *Nat. Nanotechnol.*, 2009, **4**, 249–254.
49 Y. Zhang, S. Tsitkov and H. Hess, *Nat. Commun.*, 2016, **7**, 13982.
50 C. Mukai, L. Gao, J. L. Nelson, J. P. Lata, R. Cohen, L. Wu, M. M. Hinchman, M. Bergkvist, R. W. Sherwood, S. Zhang and A. J. Travis, *Angew. Chem., Int. Ed.*, 2017, **56**, 235–238.
51 Q. Fu, W. X. Li, Y. X. Yao, H. Y. Liu, H. Y. Su, D. Ma, X. K. Gu, L. M. Chen, Z. Wang, H. Zhang, B. Wang and X. H. Bao, *Science*, 2010, **328**, 1141–1144.
52 H. Cheng, L. Zhang, J. He, W. Guo, Z. Zhou, X. Zhang, S. Nie and H. Wei, *Anal. Chem.*, 2016, **88**, 5489–5497.
53 Q. Wang, X. Zhang, L. Huang, Z. Zhang and S. Dong, *Angew. Chem., Int. Ed.*, 2017, **56**, 16082–16085.
54 C. Hou, Y. Wang, Q. Ding, L. Jiang, M. Li, W. Zhu, D. Pan, H. Zhu and M. Liu, *Nanoscale*, 2015, **7**, 18770–18779.
55 Y. Hu, H. Cheng, X. Zhao, J. Wu, F. Muhammad, S. Lin, J. He, L. Zhou, C. Zhang, Y. Deng, P. Wang, Z. Zhou, S. Nie and H. Wei, *ACS Nano*, 2017, **11**, 5558–5566.

 This journal is © The Royal Society of Chemistry 2018

Published on 13 March 2018. Downloaded by NANJING UNIVERSITY on 22/04/2018 09:59:00.

56 X. Zhou, S. Guo, J. Gao, J. Zhao, S. Xue and W. Xu, *Biosens. Bioelectron.*, 2017, **98**, 83–90.
57 M. Huo, L. Wang, Y. Chen and J. Shi, *Nat. Commun.*, 2017, **8**, 357.
58 M. I. Kim, J. Shim, T. Li, J. Lee and H. G. Park, *Chem. – Eur. J.*, 2011, **17**, 10700–10707.
59 M. I. Kim, Y. Ye, B. Y. Won, S. Shin, J. Lee and H. G. Park, *Adv. Funct. Mater.*, 2011, **21**, 2868–2875.
60 J. Yu, J. Tu, F. Zhao and B. Zeng, *J. Solid State Electrochem.*, 2010, **14**, 1595–1600.
61 J. Lee, D. Lee, E. Oh, J. Kim, Y.-P. Kim, S. Jin, H.-S. Kim, Y. Hwang, J. H. Kwak, J.-G. Park, C.-H. Shin, J. Kim and T. Hyeon, *Angew. Chem., Int. Ed.*, 2005, **44**, 7427–7432.
62 Y. Lin, L. Wu, Y. Huang, J. Ren and X. Qu, *Chem. Sci.*, 2015, **6**, 1272–1276.
63 Y. Huang, Y. Lin, X. Ran, J. Ren and X. Qu, *Chem. – Eur. J.*, 2016, **22**, 5705–5711.
64 Y. M. Ye, L. L. Xiao, B. He, Q. Zhang, T. Nie, X. R. Yang, D. B. Wu, H. L. Cheng, P. Li and Q. G. Wang, *J. Mater. Chem. B*, 2017, **5**, 1518–1524.
65 K. Qu, P. Shi, J. Ren and X. Qu, *Chem. – Eur. J.*, 2014, **20**, 7501–7506.
66 Y. Huang, Z. Liu, C. Liu, E. Ju, Y. Zhang, J. Ren and X. Qu, *Angew. Chem., Int. Ed.*, 2016, **55**, 6646–6650.
67 Y. Liu, M. Yuan, L. Qiao and R. Guo, *Biosens. Bioelectron.*, 2014, **52**, 391–396.
68 C.-J. Yu, C.-Y. Lin, C.-H. Liu, T.-L. Cheng and W.-L. Tseng, *Biosens. Bioelectron.*, 2010, **26**, 913–917.
69 C.-H. Liu and W.-L. Tseng, *Anal. Chim. Acta*, 2011, **703**, 87–93.
70 Y. Huang, M. Zhao, S. Han, Z. Lai, J. Yang, C. Tan, Q. Ma, Q. Lu, J. Chen, X. Zhang, Z. Zhang, B. Li, B. Chen, Y. Zong and H. Zhang, *Adv. Mater.*, 2017, **29**, 1700102.
71 X. He, L. Tan, D. Chen, X. Wu, X. Ren, Y. Zhang, X. Meng and F. Tang, *Chem. Commun.*, 2013, **49**, 4643–4645.
72 H. Liang, B. Liu, Q. Yuan and J. Liu, *ACS Appl. Mater. Interfaces*, 2016, **8**, 15615–15622.
73 Q. Chang and H. Tang, *Microchim. Acta*, 2014, **181**, 527–534.
74 Y. Zhao, Y. C. Huang, H. Zhu, Q. Q. Zhu and Y. S. Xia, *J. Am. Chem. Soc.*, 2016, **138**, 16645–16654.
75 K. Fan, H. Wang, J. Xi, Q. Liu, X. Meng, D. Duan, L. Gao and X. Yan, *Chem. Commun.*, 2017, **53**, 424–427.
76 Z. Zhang, X. Zhang, B. Liu and J. Liu, *J. Am. Chem. Soc.*, 2017, **139**, 5412–5419.
77 Y. Jiang, P. Arounleut, S. Rheiner, Y. Bae, A. V. Kabanov, C. Milligan and D. S. Manickam, *J. Controlled Release*, 2016, **231**, 38–49.
78 S. Shibuya, Y. Ozawa, K. Watanabe, N. Izuo, T. Toda, K. Yokote and T. Shimizu, *PLoS One*, 2014, **9**, e109288.